JOURNAL OF PROPULSION AND POWER
Vol. 25, No. 3, May–June 2009

Passive Control of Pressure Oscillations in Solid Rocket Motors: Cold-Flow Experiments

J. Anthoine* and M. R. Lema†
von Kármán Institute for Fluid Dynamics, 1640 Rhode-St-Genèse, Belgium

DOI: 10.2514/1.39794

Cold-gas experiments are used to study the pressure oscillations occurring in solid rocket motors and the performance of different ways of passive control of these oscillations. Previous studies stated that flow-acoustic coupling is mainly observed for nozzles including a cavity. The nozzle geometry has an effect on the pressure oscillations through a coupling between the acoustic fluctuations induced by the cavity volume and the vortices traveling in front of the cavity entrance. An important reduction of pressure oscillations (1 order of magnitude) is obtained, both for the axial and radial flow injection configurations, by removing the cavity located around the nozzle head. However, the nozzle integration cannot be avoided and this solution then cannot be implemented on a real flight. A permeable membrane (with holes to allow the combustion gas to pass through) placed in front of the cavity allows a reduction by a factor 1.5. The Helmholtz resonator shows a small attenuation of the pressure oscillations; however, its design could be optimized to maximize the acoustic damping. The three-dimensional-shaped inhibitors show a good attenuation of the pressure fluctuations, especially when the opening cross section is increased. This increase results in a shift of the Mach number associated with excitation. For a similar cross section, the asymmetric inhibitor (crenel-shaped) provides a reduction of pressure oscillations by a factor of 2 compared with an axisymmetric inhibitor. Therefore, the asymmetry of the inhibitor seems to be the best candidate for reducing the pressure oscillations.

Nomenclature

c_0	=	sound speed
D	=	internal diameter of the model
d	=	internal diameter of the inhibitor
f	=	frequency of the oscillation
He	=	Helmholtz number
j	=	excited acoustic-mode number
L	=	total length
l	=	inhibitor-nozzle distance
M_0	=	mean Mach number
m	=	stage number
P_{rms}	=	oscillatory pressure
P_s	=	mean static pressure
S	=	model cross surface
V_c	=	nozzle cavity volume
γ	=	ratio of specific heats

Subscripts

ac	=	acoustic
j	=	acoustic-mode number

Introduction

THE present research is an experimental investigation of the aeroacoustic instabilities occurring in a subscaled cold-flow model of the Ariane 5 solid rocket motor. The phenomenon develops in the confined flow established in the motor and involves a coupling between hydrodynamic instabilities and longitudinal acoustic modes.

Aeroacoustic instabilities occur in a wide range of technical applications. The resulting oscillations are sometimes wanted in systems designed to produce the periodic motion efficiently, such as in musical instruments. Nevertheless, in most cases, aeroacoustic instabilities perturb the operation, as for the Ariane 5 launcher. The present research investigates the aeroacoustic instabilities that lead to pressure and thrust oscillations, which reduce the rocket motor performances and could damage the payload.

Previous Studies

For technological reasons, large solid rocket motors (SRMs) are composed of a submerged nozzle and segmented propellant grains separated by inhibitors (Fig. 1). During propellant combustion, a cavity appears around the nozzle. Vortical flow structures may be formed from the downstream inhibitor [obstacle vortex shedding (OVS)] or from natural instabilities of the radial flow resulting from the propellant combustion [surface vortex shedding (SVS)]. Flandro and Majdalani [1] use this concept of SVS to explain the instabilities in existing SRMs that do not have inhibitors. Chedevergne et al. [2] develop a stability analysis of the flow induced by wall injection. The hydrodynamic manifestations drive pressure oscillations in the internal flow established in the motor. When the vortex-shedding frequency synchronizes acoustic modes of the motor chamber, resonance may occur and sound pressure can be amplified by vortex–nozzle interaction, leading to pressure and thrust oscillations.

The stability prevision of large solid rocket motors has been an active subject, both in the United States and in Europe, in the past 25 years. Although these motors were predicted to be stable by classical stability-assessment methods [3,4], such grain segmentation conducted to low-amplitude, but sustained, pressure and thrust oscillations on first longitudinal acoustic-mode frequencies. These pressure oscillations have been reported for the space shuttle redesigned solid rocket motor (RSRM), the Titan-34D SRM, the Titan-IV solid rocket motor upgrade (SRMU), and the Ariane 5 moteur à propergol solide (MPS) [4–8]. All of these boosters have a length-to-diameter ratio (L/D) in the range of 9–12 and demonstrate similar pressure oscillations, whatever the number of segments.

Presented as Paper 4602 at the 44th AIAA/ASME/SAE/ASEE Joint Propulsion Conference and Exhibit, Hartford, CT, 21–23 August 2008; received 15 July 2008; revision received 24 July 2008; accepted for publication 17 September 2008.

*Associate Professor, Environmental and Applied Fluid Dynamics Department, Chaussée de Waterloo 72; anthoine@vki.ac.be. Senior Member AIAA.

†Research Engineer, Environmental and Applied Fluid Dynamics Department, Chaussée de Waterloo 72.

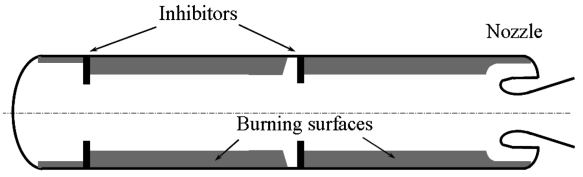

Fig. 1 Internal geometry of the Ariane 5 SRM.

Zero-peak relative amplitudes are typically less than 0.5% for pressure oscillations and less than 5% for thrust oscillations. Similar results were also observed on subscaled model rockets [9,10] and from numerical simulations [11–14]. The use of three-dimensional inhibitors to reduce the pressure oscillations was already tested and simulated by Telara et al. [15].

From cold-flow experiments in a pipe with one or two inhibitors, Culick and Magiawala [16], Dunlap and Brown [17], Mettenleiter et al. [18], and Anthoine [19] showed that the vortex shedding is produced at the inhibitors, and the confined space of the pipe acts as a resonator with its natural frequencies. Pressure oscillation reaches a large amplitude when the vortex-shedding frequency is close to the frequency of one resonant acoustic mode of the system. Culick and Magiawala [16] showed that it was impossible to sustain acoustic modes with only one inhibitor. The presence of an obstacle downstream of the shedding point of the vortices provides the necessary acoustical feedback when the vortices interact with it [20,21]. In the case of segmented rocket motors, this second obstacle is the nozzle.

The development of original analytical models to point out the parameters controlling the flow-acoustic coupling (see the next section) and the effect of the nozzle design on sound production (nonlinear model), was already presented, as well as their validation with experimental data [19,22]. The nonlinear model based on vortex-sound theory stated that flow-acoustic coupling is mainly observed for nozzles including a cavity. The nozzle geometry has an effect on the pressure oscillations through a coupling between the acoustic fluctuations induced by the cavity volume and the vortices traveling in front of the cavity entrance. When resonance occurs, the sound pressure level P_{rms}/P_s increases linearly with the chamber Mach number M_0, the excited mode number j, and the nozzle cavity volume V_c:

$$\frac{P_{\text{rms}}}{P_s} \sim \frac{\pi\gamma}{\gamma - 1} j M_0 \frac{V_c}{V_{\text{tot}}} \tag{1}$$

where

$$V_{\text{tot}} = \frac{\pi D^2}{4} L \tag{2}$$

In the absence of a cavity, the pressure fluctuations are damped.

Experimental Facilities

The experiments are conducted on 1/30-scale axisymmetric cold-flow models, respecting the Mach number similarity with the Ariane 5 SRM when 50% of the propellant is burned [23–26]. That midcombustion condition corresponds to the maximum of pulsations. The Mach number based on the mean flow velocity in the segments is of the order of 0.1. Because the Reynolds number based on the same velocity and on the segments diameter is of the order of 2×10^7 in the full-scale motor, the viscous effects are negligible and do not influence the flow properties. Therefore, exact Reynolds number scaling is not required as long as it is large enough.

The flow is either created by an axial air injection at the forward end (Fig. 2a) or by a radial injection uniformly distributed along the chamber's porous cylinders (Fig. 2b). The cold air is injected in the model through porous materials and the acoustic insulation of the test section from the air supply is checked. Each test section includes only one inhibitor and a submerged nozzle. The main characteristic of the submerged nozzle is the appearance of a cavity around its convergent part.

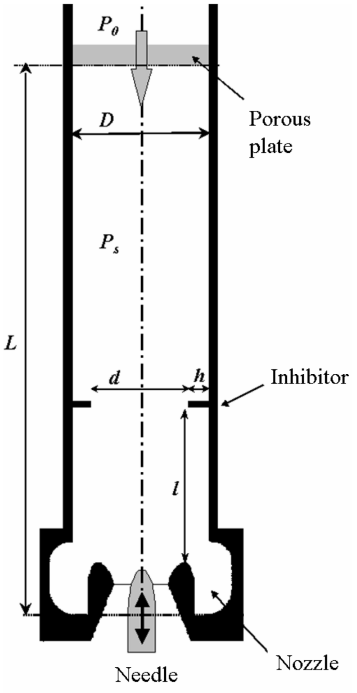

a) Axial injection

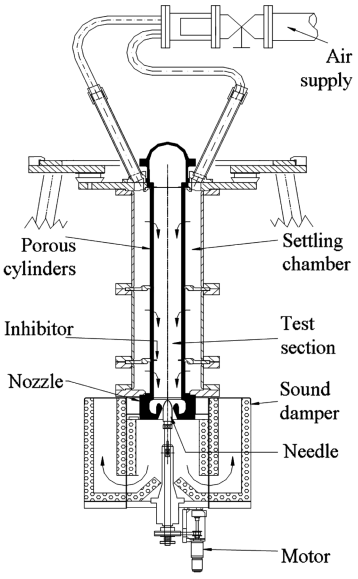

b) Radial injection

Fig. 2 Axial and radial cold-flow setups (1/30 scale).

With the radial setup, tests can also be made without an inhibitor to simulate the SVS. Experiments proved that the radial injection through porous cylinders correctly simulates the Taylor flow and the combustion situation [19,26]. Experimental velocity spectra demonstrated that the flow is stable near the forward end until it reaches a critical axial position. Then the flow becomes unstable downstream for a range of frequencies that increases with the distance from the forward end. Therefore, vortices are issued from the hydrodynamic instability of the radial injection (SVS).

The two test sections allow a wide range of parameters to be tested, such as the total length, the inhibitor shape and the nozzle geometry. The internal Mach number can be varied continuously by means of a movable needle placed in the nozzle throat. The acoustic pressure measurements are performed by piezoelectric transducers, and signal treatment yields the amplitude and the frequency of the pressure oscillations. The frequency resolution is smaller than 1 Hz.

Identification of Flow-Acoustic Coupling

Flow-acoustic coupling is identified by plotting the evolution of the maximum pressure fluctuation, in terms of frequency and amplitude, versus Mach number. Figure 3a shows the pressure-fluctuation spectrum plotted versus Mach number M_0 and frequency f for the axial flow injection configuration with an inhibitor of 58 mm internal diameter placed 71 mm from the head of the submerged nozzle. Oscillation frequencies f are close to the resonance frequencies characterized by $f_{\mathrm{ac},j} = jc_0/(2L)$, because the acoustic standing wave can be modeled in first approximation by that of a closed–closed pipe segment of length L. In the Mach number range between 0.072 and 0.082, the frequency of the peak ($f = 850$ Hz) is very close to the second longitudinal acoustic-mode frequency of the test section, estimated by $f_{\mathrm{ac},2} = c_0/L$ ($c_0 = 338$ m/s and $L = 0.393$ m). The oscillation frequency seems to vary slowly and linearly with the Mach number. This change takes care for the necessary phase shift needed to compensate for the change in travel time of vortical structures that is needed to obtain a phase shift equal to an integer number of 2π along the feedback loop. This phenomena has been extensively described for deep cavities [27,28] and the flute [29,30]. We will therefore call this a flute behavior.

Figure 3a can also be plotted in term of Helmholtz number $He = fl/c_0$ instead of frequency f. As l and c_0 are constant, He is a nondimensional representation of the pressure-fluctuation frequency. The maximum of the pressure-fluctuation values are plotted versus Mach number in Fig. 3b. The evolution of the Helmholtz number corresponding to the maximum of the pressure fluctuations is also given in Fig. 3b. In such a plot, the longitudinal acoustic modes of the test section characterized by $He_{\mathrm{ac},j} = jl/(2L)$ correspond to horizontal lines. For such test conditions, each time the excited frequency is close to an acoustic-mode frequency, the pressure-fluctuation level is large. The maximum is reached when it crosses the acoustic mode.

Figures 4a and 4b provide the same information as Fig. 3a for the radial flow injection configuration with an inhibitor placed in the middle of the test section (OVS/SVS) and without an inhibitor (only SVS).

Flow-acoustic coupling stands up when the vortex-shedding frequency is equal to the acoustic-mode frequency. There is a lock-on phenomenon of the vortex-shedding frequency that jumps between the acoustic modes. At resonance, the pressure spectra show excitation of the first two longitudinal acoustic modes for the axial flow injection (OVS), successive long excitations of the second and then third modes for the radial flow injection with an inhibitor (OVS/SVS), and multiple successive short excitations of the first and then second longitudinal modes for the radial flow injection without an inhibitor (SVS). The terms *long* and *short* refer to the size of the range of Mach number of each individual excitation. In all

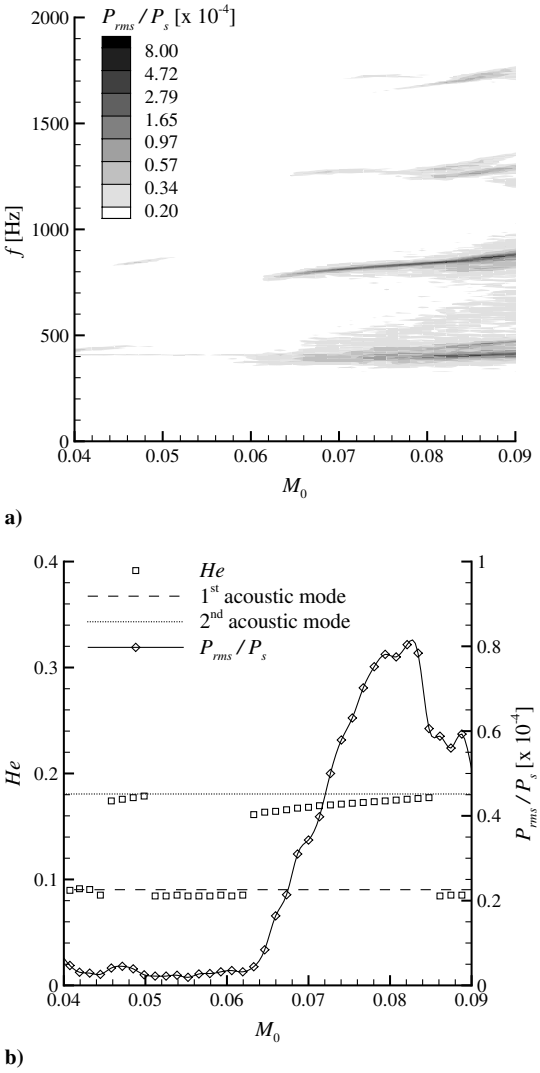

Fig. 3 Plots of a) contours of pressure fluctuations in terms of frequency and amplitude and b) evolution of the maximum of the pressure fluctuation in terms of Helmholtz number and amplitude; axial flow injection; $L = 393$ mm, $l = 71$ mm, and $d = 58$ mm; submerged nozzle.

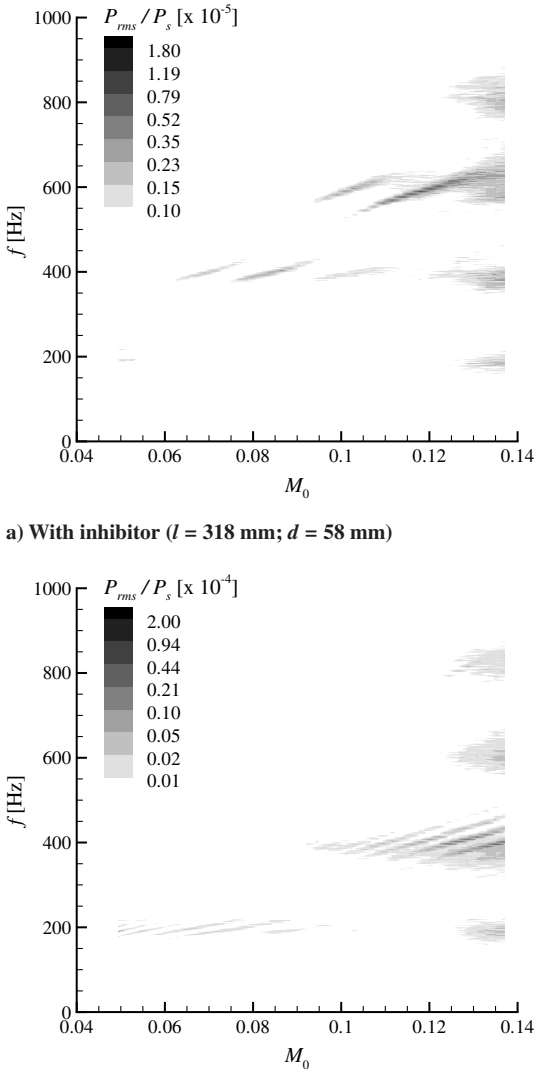

Fig. 4 Contours of pressure fluctuations in terms of frequency and amplitude; radial flow injection; $L = 792$ mm; submerged nozzle.

configurations, the sound pressure level reached under resonant condition results from a vortex–nozzle interaction. The vortices impinge on the nozzle head more coherently and feed energy into one mode of the system, bringing the fluctuation level to a larger value. The geometrical parameters such as the inhibitor-nozzle distance, the total length, the inhibitor inner diameter, and the test-section inner diameter select the acoustic modes to be excited, the number of vortices present between the shedding point and the nozzle, and the internal Mach number of excitation.

It is worth attempting to derive an analytical model to predict the conditions for the occurrence of flow-acoustic coupling. This model is based on Rossiter's [31] approach. The generation of self-sustained sound resonance in a tube depends on the phase of the acoustic oscillation at which a vortex shed by the upstream obstacle reaches the downstream obstacle [32]. In the present model, the upstream obstacle is the inhibitor and the downstream obstacle is the nozzle. Finally, flow-acoustic coupling occurs at the following Mach number:

$$M_0 = \frac{C_{vc}}{2k_v}\frac{j}{m - 0.25}\frac{l}{L}\left(\frac{d}{D}\right)^2 \tag{3}$$

where C_{vc} is the vena contracta coefficient of the jet generated by the inhibitor [33], and k_v is the ratio of the vortex transport velocity to the jet velocity. From the experimental investigation of the vortex properties [19], $C_{vc} = 0.68$ and $k_v = 0.47$.

When resonance occurs, the selection of the acoustic mode j depends on the relative position l/L of the inhibitor compared with the acoustic-mode shape. Indeed, to yield high sound pressure levels and to obtain a maximum of acoustic receptivity at the inhibitor, the inhibitor must be as close as possible to an acoustic pressure node (highest acoustic velocity fluctuations). Then the coupling will occur for that acoustic mode only when an integer number of vortices m are present between the inhibitor and the nozzle. The flow-acoustic coupling will excite that acoustic mode with that number of vortices only for some Mach number M_0, depending on the geometrical parameters (l/L and d/D), so that relation 3 is respected.

Looking at Fig. 3b, the maximum of the sound pressure level is observed experimentally to excite the second mode at a Mach number M_0 equal to 0.082. The inhibitor is placed at 26% from the end of the test section. Then the excited mode j will preferably be the second longitudinal acoustic mode. From Eq. (3), a flow-acoustic coupling is predicted to occur at a Mach number equal to 0.086 with $m = 2$ vortices located between the inhibitor and the nozzle. Such a finding is also in good agreement with numerical simulations [13] and experimental observation obtained from particle image velocimetry measurements [34].

Nozzle Design Modification as a Control of Pressure Oscillations

The modification of the nozzle design has been tested for both axial and radial flow configurations. As indicated by the original analytical model [Eq. (1)], the nozzle geometry is expected to play an important role in the amplification of the sound pressure fluctuations. Indeed, by changing the nozzle design, the downstream obstacle (on which the vortices impinge, generating the acoustic waves) is modified, as is the flowfield around the nozzle. However, the main reason for the nozzle effect is the cavity volume around the nozzle. The compressibility of the air in that cavity volume induces an acoustical velocity at the cavity entrance that interacts with the vortices when they are passing just in front of the cavity entrance, generating noise.

Several nozzle geometries have been compared for both axial and radial flow injection. For all nozzles, the convergent and divergent parts have the same profiles: only the cavity geometry is changed by filling it. Note that when filling the cavity, the effective total length of the test section L is also slightly changing and the acoustic-mode frequencies are modified accordingly. Figure 5a shows the evolution of the maximum of the pressure fluctuations for four different nozzles and for an inhibitor-nozzle distance of 71 mm for the axial flow configuration (OVS). The evolution of the Helmholtz number, not shown here, is similar for all of the nozzles except for nozzle 4 (without a cavity). It means that the vortex shedding does excite the second longitudinal acoustic-mode within the same Mach number range for all of the nozzles except for nozzle 4, for which there is no mode excitation. The maximum of sound pressure level that corresponds to the maximum of coupling appears at $M_0 = 0.08$, whatever the nozzle geometry. But the amplitude of the maximum resonance is highly dependent on the nozzle design. When the nozzle cavity volume decreases (from nozzle 1 to 2), the pressure fluctuation drops. The effect of the nozzle head geometry is shown by nozzle 3. This nozzle presents a smaller cavity volume than nozzle 2, which results in fainter pressure fluctuations than with nozzle 2. Finally, the nozzle without a cavity (nozzle 4) shows pressure levels reduced by a factor 10, compared with nozzle 1.

The effect of the nozzle cavity volume on the amplification of the pressure fluctuations occurring on the second acoustic mode at $M_0 = 0.08$ is summarized in Fig. 5b for the axial flow configuration. The evolution of the maximum sound pressure level is approximately linear with the nozzle cavity volume. Such a result compares well with the analytical model developed on purpose [Eq. (1)].

Figures 6a and 6b provide the comparison of pressure oscillations with and without a cavity around the nozzle for the radial flow

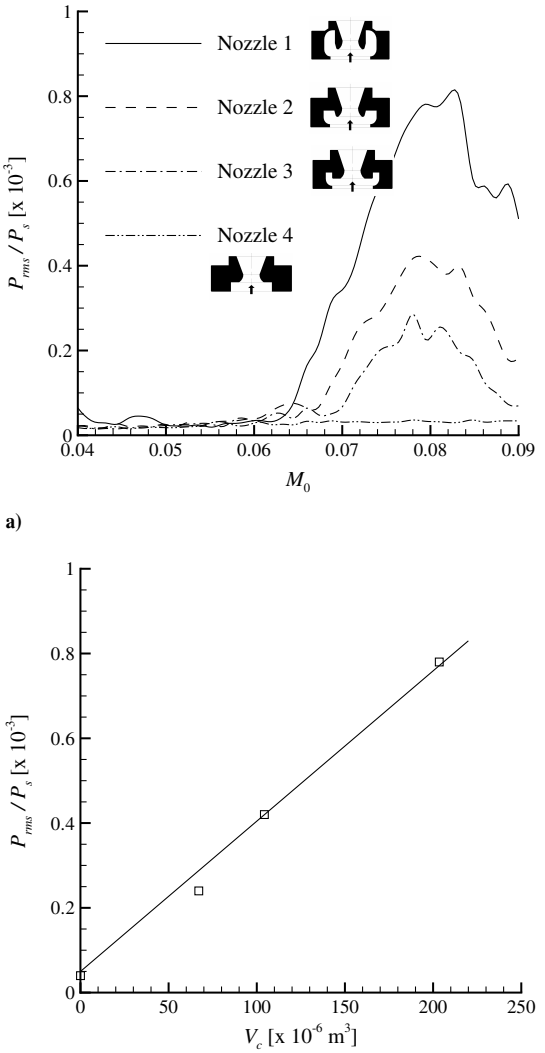

Fig. 5 Plots of a) pressure oscillations for different nozzle geometries and b) effect of nozzle cavity volume on pressure levels for the axial flow configuration; $L \sim 390$ mm, $l = 71$ mm, and $d = 58$ mm.

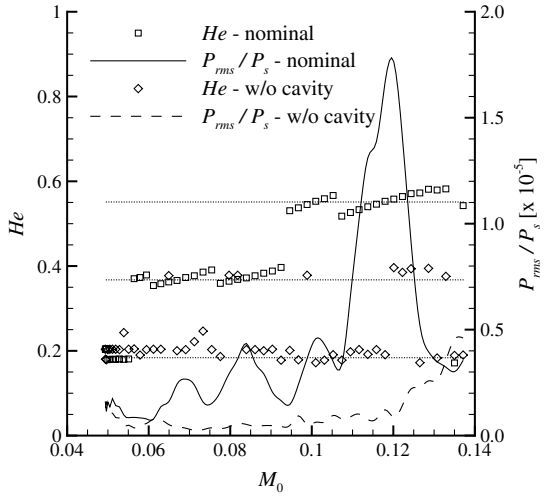

a) With inhibitor (l=318 mm; d=58 mm)

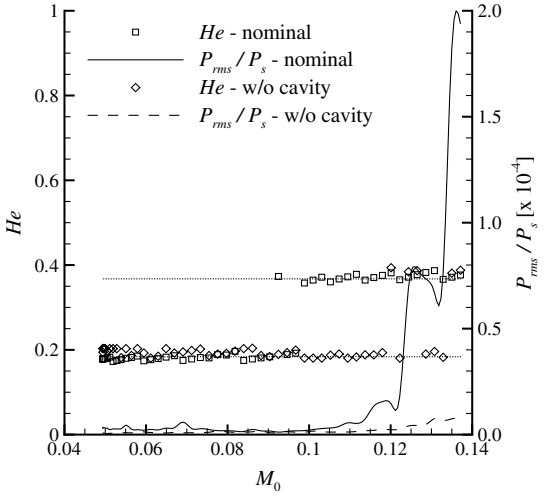

b) Without inhibitor

Fig. 6 Pressure oscillations for different nozzle geometries for the radial flow configuration; $L \sim 790$ mm.

injection configuration with an inhibitor placed in the middle of the test section (OVS/SVS) and without an inhibitor (only SVS), respectively. The nozzle design also has an effect on the amplitude of the pressure oscillations in the case of radial flow injection. It has been shown that pressure oscillations are coming from a coupling between the acoustic fluctuations induced by the cavity volume and the vortices traveling in front of the cavity entrance. Therefore, the best solution for passive control of the pressure oscillations is to replace the submerged nozzle by a nonintegrated nozzle (without a cavity). However, in practice, this integration is needed for the rocket thrust control. For evident practical reasons, it is then not possible to remove the integration.

Other Passive Ways to Control Pressure Oscillations

Control of pressure oscillations by passive ways remains the only possibility of improving the SRM performance. The following passive ways are only tested for the axial flow configuration (OVS). Three kinds of passive control systems are explored: insertion of a membrane (impermeable or permeable) in front of the cavity entrance to prevent vortex–nozzle interaction, installation of a resonator (Helmholtz resonator or quarter wavelength tube) to damp the pressure oscillations, and modification of the inhibitor geometry (three-dimensional-shaped, outlying) to reduce the vortex coherence.

Insertion of a Membrane

The idea is to prevent the vortices from interacting with the nozzle cavity while passing in front of the cavity entrance by inserting a solid membrane at the entrance of the cavity. The first membrane to be tested is completely impermeable (Fig. 7b) and is expected to completely damp the pressure oscillations, because the flow-acoustic coupling should disappear. In fact, the results should be similar to those obtained without a cavity at the nozzle. This membrane is then the best solution for passive control of an integrated nozzle. However, using a solid membrane, the integrated nozzle cannot be surrounded by propellant. The last propellant grain should be between the inhibitor and the membrane. This will result in a reduction of the performance of the launcher, because the ratio of propellant mass to inert mass is reduced.

To overcome this problem of propellant mass reduction, the next idea is to use a permeable membrane for passive control (Fig. 7c). That membrane presents 16 small circular holes through which the flow coming from the propellant combustion can exit the nozzle cavity. The diameter of the holes is equal to 6 mm. The motor performance should not be affected by this membrane but the vortices are still able to interact with the acoustic fluctuations induced by the cavity volume. It is, however, expected that this interaction will be weaker than without a membrane, producing smaller pressure oscillations.

Pressure fluctuations are measured for an inhibitor with $d = 58$ mm placed at $l = 71$ mm from the head of the submerged nozzle. The maximum of the pressure fluctuation is plotted versus Mach number for the different test cases in Fig. 8.

The maximum sound pressure levels that correspond to a coupling on the second acoustic mode appear at $M_0 = 0.08$, but the amplitude of the maximum resonance is influenced by the use of passive control. As expected, the passive control with impermeable membrane produces the same pressure oscillations as when the cavity is not present (so a reduction by a factor of about 10). This proves again that the pressure oscillations are induced by the presence of the cavity, through a coupling between the acoustic fluctuations induced

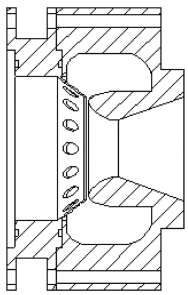

a) Installation of the membrane

b) Impermeable

c) Permeable

Fig. 7 Geometries of the membranes.

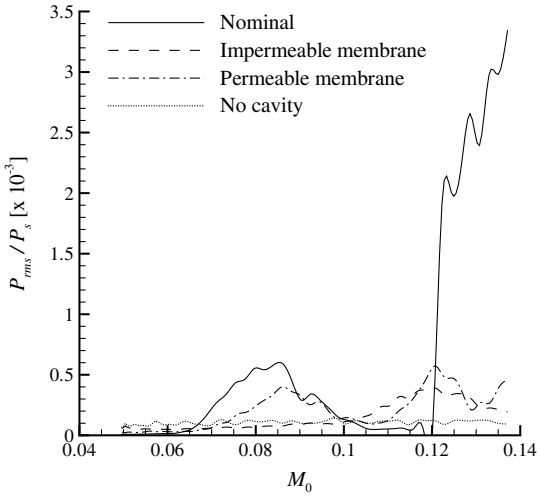

Fig. 8 Evolution of the maximum pressure oscillations for different membranes placed in front of the nozzle entrance; $l = 71$ mm and $d = 58$ mm.

by the cavity volume and the vortices traveling in front of the cavity entrance, as already explained through the analytical model.

However, the use of an impermeable membrane results in a reduction of the performance of the launcher, as explained before. With the permeable membrane, the attenuation of the pressure oscillations is less than without a cavity or with the impermeable membrane. Looking to the excitation of the second mode around $M_0 = 0.08$, the pressure oscillations are weaker by a factor of 1.5 (attenuation factor of 0.67), compared with the submerged nozzle without a membrane.

The analytical model (relation 1) is adapted for the passive control with a permeable membrane to determine the attenuation factor of the pressure oscillations. The difference from what was done previously [22] is that the cross surface of the cavity entrance is reduced to the section of the 16 holes in the permeable membrane, and the mean distance over which the vortex travels in front of the cavity entrance is reduced to the mean distance in the vortex-path direction over the hole cross surface. When using the permeable membrane, the attenuation factor of the pressure oscillations is given by

$$\frac{P_{\text{rms,control}}}{P_{\text{rms,no control}}} \sim \frac{\pi}{4} \tag{4}$$

which is very close to the measured attenuation factor of 0.67.

Installation of a Resonator

Resonators are acoustical elements used to attenuate the sound at narrowband frequencies in both ducts and tubes. A simple resonator comprises a cavity enclosing a mass of air, with a narrow opening to the outside, called the neck. In this way, the mass of air effectively acts as a spring at the resonant frequency of the cavity and, under those conditions, absorbs appreciable sound energy, exciting the resonance.

The considered resonator is of the Helmholtz type and is placed at the forward end to coincide with a pressure antinode. The resonant frequency of the Helmholtz resonator is given by

$$f_r = \frac{c_0}{2\pi}\sqrt{\frac{S_r}{V_r(l_r + 2\delta)}} \tag{5}$$

where V_r is the volume of the resonator cavity, S_r is the neck cross section, and l_r is the neck length. The correction factor δ depends on the radius of the neck, r:

$$2\delta = 1.7r \tag{6}$$

The transmission coefficient of this resonator can be calculated using the following equation [35]:

$$\alpha_t = 1 \Big/ \left(1 + \frac{c_0^2}{4S^2[2\pi f_r(l_r + 2\delta/S_r) - (c_0^2/2\pi f_r V_r)]^2}\right) \tag{7}$$

This transmission coefficient becomes zero at the resonance frequency, as plotted in Fig. 9a. At this frequency, large velocity amplitudes exist in the neck of the resonator, and all acoustic energy transmitted into the resonator cavity from the incident wave is returned to the main pipe, with such a phase relationship as to be reflected back toward the source.

The evolution of the pressure-fluctuation amplitude and Helmholtz number as a function of the Mach number is presented in Fig. 9b and compared with the data of the nominal configuration (without resonator). At the frequency of the second acoustic mode, the maximum pressure fluctuations are attenuated by a factor of 2. However, even though the attenuation is good, the range of frequency at which the Helmholtz resonator is effective is very narrow. As plotted in Fig. 9a, an attenuation of at least 30% is obtained between 860 and 890 Hz, which corresponds to a frequency bandwidth of 30 Hz. As can be observed in Fig. 3a, the evolution of the frequency with Mach number during the acoustic coupling is approximately linear with a slope of 3000 Hz/Mach. Therefore, a

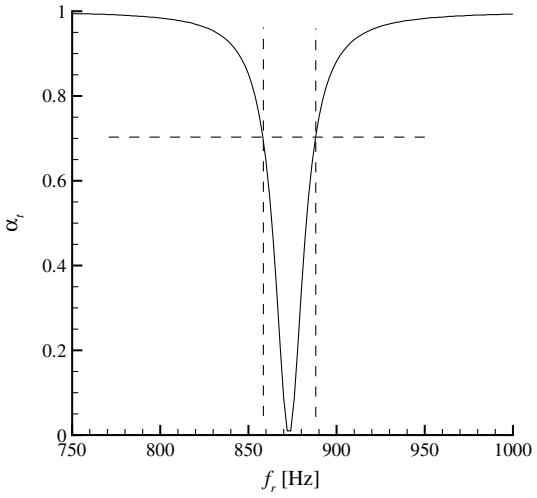

a) Attenuation coeffcient

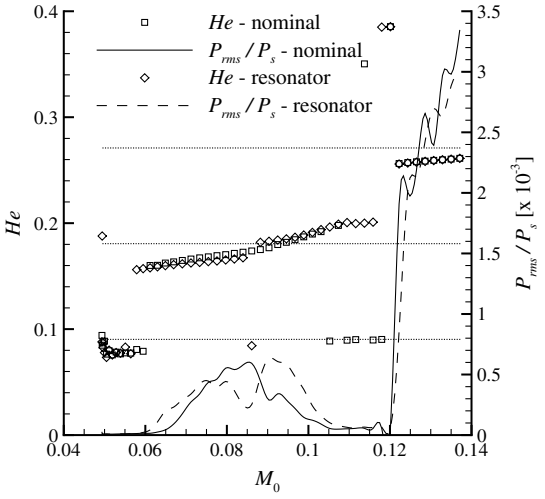

b) Pressure oscillations

Fig. 9 Attenuation coefficient of the Helmholtz resonator and evolution of the maximum pressure oscillations with resonator; $l = 71$ mm and $d = 58$ mm.

frequency bandwidth of 30 Hz corresponds to a Mach range of 0.01. This is fully coherent with the results of Fig. 9b, in which the Helmholtz resonator proves to be efficient in the Mach number range between 0.08 and 0.09. The frequency bandwidth at which the resonator is effective can be modified by changing the resonator cavity and the neck dimensions, but with the disadvantages of a higher transmission coefficient, which means that the resonator attenuates a wider range of frequencies, but less effectively. Therefore, the resonators are not providing the best control performance; however, they could be optimized.

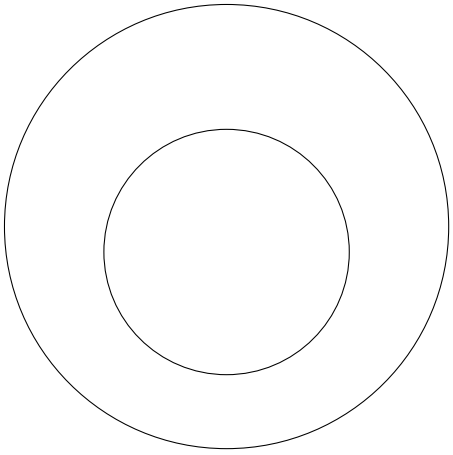

a) Outlying opening

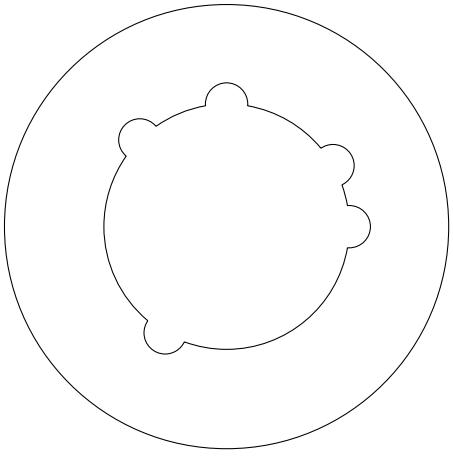

b) Axisymmetric opening but randomly drilled

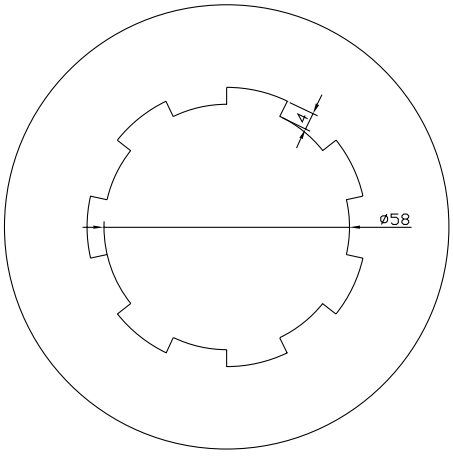

c) Crenel-shaped opening (same diameter)

Fig. 10 Three-dimensional-shaped inhibitors.

Modification of the Inhibitor Geometry

The final way to reduce the pressure oscillations consists of destroying the coherence of the vortices before they reach the nozzle, which is possible by modifying the inhibitor geometry. The nominal geometry is annular, but other geometries are considered: an inhibitor of diameter $d = 58$ mm with an outlying opening (center shifted by 5.5 mm), an inhibitor with an axisymmetric opening ($d = 58$ mm) but randomly drilled at five locations, and an inhibitor with a crenel-shaped opening section ($d = 58$ mm) made of seven crenel cuts (Fig. 10).

The pressure fluctuations are measured for these 3-D-shaped inhibitors placed at $l = 71$ mm from the head of the submerged nozzle. Figure 11 shows the evolution of the maximum of the pressure fluctuations for the different 3-D-shaped inhibitors. The nominal case (axisymmetric inhibitor with $d = 58$ mm) and the axisymmetric inhibitor with $d = 62$ mm are also shown in Fig. 11.

For the inhibitor with an outlying opening, the level of pressure fluctuations lessens. The height h of that inhibitor varies from 3.5 to 14.5 mm, but has the same influence on the frequency and pressure levels as decreasing the inhibitor height in the complete perimeter, as happens for the inhibitor of 68 mm (not shown here) [19], in which the height h is constant and equal to 4 mm. The outlying opening of the inhibitor open area seems to be a very good candidate for passive control.

The cross section of the inhibitor with an axisymmetric opening (but randomly drilled) is increased, which results in a shift of the Mach number range, compared with the nominal case (Fig. 11). This shift was already found analytically in relation 3. From relation 1, the pressure oscillations are linearly proportional to the Mach number. Therefore, a shift of the Mach number should be associated with an increase of the pressure oscillations, whereas the pressure-level amplitude associated with the randomly drilled inhibitor is slightly decreased. Therefore, the asymmetric shape of the drilled inhibitor allows reducing the pressure-level amplitude.

Regarding the crenel-shaped inhibitor with the same inner diameter as the nominal case, the conclusions are similar to those for the drilled inhibitor (Fig. 11). The evolution of the maximum of the pressure fluctuations for the crenel-shaped inhibitor is similar to, but with a lower amplitude than, that obtained with an axisymmetric inhibitor of 62 mm inner diameter (Fig. 11). In both cases, the excitation appears on the second acoustic mode and at the same Mach number ($M_0 = 0.11$), but for a higher Mach number than with the nominal case, due to the increase of the cross section. It is then possible to deduce from these two tests the effective reduction of the pressure oscillations due to the dissymmetry of the inhibitor: that reduction is equal to 48%.

These results also confirmed that, as expected from relation 3, the increase of the cross section of the inhibitor is associated with a proportional shift of the Mach number, as plotted in Fig. 12. The

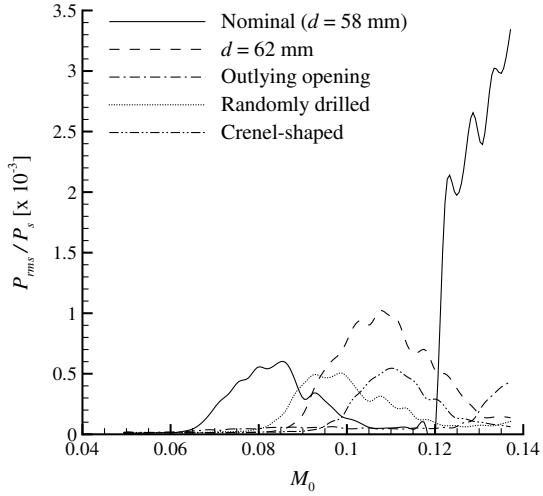

Fig. 11 Pressure oscillations with 3-D-shaped inhibitors; submerged nozzle; $l = 71$ mm.

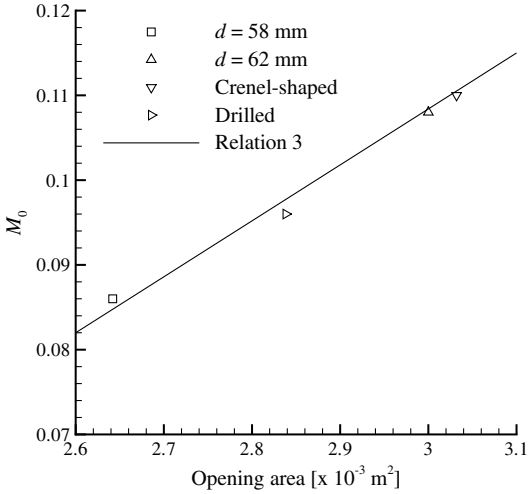

Fig. 12 Evolution of the Mach number that crosses the second acoustic mode versus the opening area of different inhibitors.

Mach number that crosses the second acoustic mode versus the opening area follows a linear evolution; therefore, if the opening area of the inhibitor is higher than 3.6×10^{-3} m^2, the second longitudinal mode of the present setup is not excited.

In conclusion, the asymmetry of the inhibitor provides a promising way of reducing the pressure oscillations. A further parametric investigation is needed to determine the influence of the inhibitor shape parameters (type of asymmetry, number and height of the crenel cuts, etc.) and to deduce the optimal shape.

Conclusions

This paper addressed different ways of passive control of pressure oscillations in SRM and their performances in cold-gas conditions. The most important reduction of pressure oscillations is obtained by removing the cavity located around the nozzle head or adding an impermeable membrane in front of the nozzle cavity. This has been proved to be a very good solution for both the axial and radial flow injection configurations, with reductions by a factor up to 10. However, because the nozzle integration cannot be avoided and the impermeable membrane will reduce the motor performance, neither of these two solutions can be implemented on a real flight. A permeable membrane (with holes to allow the combustion gas to pass through) allows a reduction by a factor of 1.5. The Helmholtz resonator shows a small attenuation of the pressure oscillations; however, its design can be optimized to maximize the acoustic damping. The 3-D-shaped inhibitors show a good attenuation of the pressure fluctuations, especially when the opening cross section is increased. This increase results in a shift of the Mach number associated with excitation. For a similar cross section, the asymmetric inhibitor (crenel-shaped) provides a reduction of pressure oscillations by a factor of 2, compared with an axisymmetric inhibitor. Therefore, the asymmetry of the inhibitor seems to be the best candidate for reducing the pressure oscillations.

Acknowledgments

This research has been partly supported by ESA through the Ariane-5 Research and Technology Accompaniment (ARTA) program, within ESA contract number 19581/06/F/DC. The authors would like to thank M. C. Contino and J. Steelant from ESA for their support to the von Kármán Institute research activities. The measurements using the radial flow injection setup shown in this paper have been performed and analyzed by B. Tóth.

References

[1] Flandro, G. A., and Majdalani, J., "Aeroacoustic Instability in Rockets," AIAA Paper 2001-3868, 2001.

[2] Chedevergne, F., Casalis, G., and Feraille, T., "Biglobal Linear Stability Analysis of the Flow Induced by Wall Injection," *Physics of Fluids*, Vol. 18, No. 1, 2006, Paper 014103. doi:10.1063/1.2160524

[3] Lovine, R. L., and Waugh, R. C., *Standard Stability Prediction Method for Solid Rocket Motors*, Chemical Propulsion Information Agency Rept. 273, Columbia, MD, 1975.

[4] Brown, R. S., Dunlap, R., Young, S. W., and Waugh, R. C., "Vortex Shedding as a Source of Acoustic Energy in Segmented Solid Rockets," *Journal of Spacecraft and Rockets*, Vol. 18, No. 4, 1981, pp. 312–319. doi:10.2514/3.57822

[5] Mason, D. R., Folkman, S. L., and Behring, M., "Thrust Oscillations of the Space Shuttle Solid Rocket Booster Motor During Static Tests," AIAA Paper 79–1138, 1979.

[6] Blomshield, F. S., and Mathes, H. B., "Pressure Oscillations in Post-Challenger Space Shuttle Redesigned Solid Rocket Motors," *Journal of Propulsion and Power*, Vol. 9, No. 2, 1993, pp. 217–221. doi:10.2514/3.23612

[7] Dotson, K. W., Koshigoe, S., and Pace, K. K., "Vortex Shedding in a Large Solid Rocket Motor without an inhibitors at the Segmented Interfaces," *Journal of Propulsion and Power*, Vol. 13, No. 2, 1997, pp. 197–206. doi:10.2514/2.5170

[8] Scippa, S., Pascal, P., and Zanier, F., "Ariane-5 MPS: Chamber Pressure Oscillations Full Scale Firings Results Analysis and Further Studies," AIAA Paper 94-3068, 1994.

[9] Prévost, M., Vuillot, F., and Traineau, J. C., "Vortex Shedding Driven Oscillations in a Subscale Motor for the Ariane 5 MPS Solid Rocket Motors," AIAA Paper 96-3247, 1996.

[10] Traineau, J. C., Prévost, M., Vuillot, F., Le Breton, P., Cuny, J., Preioni, N., and Bec, R., "A Subscale Test Program to Assess the Vortex Shedding Driven Instabilities in Segmented Solid Rocket Motors," AIAA Paper 97-3247, 1997.

[11] Vuillot, F., "Vortex-Shedding Phenomena in Solid Rocket Motors," *Journal of Propulsion and Power*, Vol. 11, No. 4, 1995, pp. 626–639. doi:10.2514/3.23888

[12] Mombelli, C., Guichard, A., Godfroy, F., and Guéry, J.-F., "Parallel Computation of Vortex Shedding in Solid Rocket Motors," AIAA Paper 99-2510, 1999.

[13] Anthoine, J., Buchlin, J.-M., and Guéry, J.-F., "Effect of Nozzle Cavity on Resonance in Large SRM: Numerical Simulations," *Journal of Propulsion and Power*, Vol. 19, No. 3, 2003, pp. 374–384. doi:10.2514/2.6141

[14] Cosyn, P., Vierendeels, J., and Anthoine, J., "Numerical Simulation of Aeroacoustic Phenomena in a Solid Rocket Booster," *Journal of Spacecraft and Rockets*, Vol. 42, No. 1, 2005, pp. 111–117. doi:10.2514/1.3579

[15] Telara, M., Paglia, F., Stella, F., and Giangi, M., "Ariane 5 P230 SRM Frontal Thermal Protection Evolution: Numerical Simulation," 42nd AIAA/ASME/SAE/ASEE Joint Propulsion Conference and Exhibit, Sacramento, CA, AIAA Paper 2006-5242, July 2006.

[16] Culick, F. E. C., and Magiawala, K., "Excitation of Acoustic Modes in a Chamber by Vortex Shedding," *Journal of Sound and Vibration*, Vol. 64, No. 3, 1979, pp. 455–457. doi:10.1016/0022-460X(79)90591-1

[17] Dunlap, R., and Brown, R. S., "Exploratory Experiments on Acoustic Oscillation Driven by Periodic Vortex Shedding," *AIAA Journal*, Vol. 19, No. 3, 1981, pp. 408–409. doi:10.2514/3.7783

[18] Mettenleiter, M., Haile, E., and Candel, S., "Adaptive Control of Aeroacoustic Instabilities," *Journal of Sound and Vibration*, Vol. 230, No. 4, 2000, pp. 761–789. doi:10.1006/jsvi.1999.2659

[19] Anthoine, J., "Experimental and Numerical Study of Aeroacoustic Phenomena in Large Solid Propellant Boosters," Ph.D. Thesis, Univ. Libre de Bruxelles, Brussels, Oct. 2000.

[20] Flatau, A., and VanMoorhem, W., "Prediction of Vortex Shedding Responses in Segmented Solid Rocket Motors," AIAA Paper 90-2073, 1990.

[21] Schachenmann, A., and Rockwell, D., "Self–Sustained Oscillations of Turbulent Pipe Flow Terminated by an Axisymmetric Cavity," *Journal of Sound and Vibration*, Vol. 73, No. 1, 1980, pp. 61–72. doi:10.1016/0022-460X(80)90492-7

[22] Anthoine, J., Buchlin, J.-M., and Hirschberg, A., "Effect of Nozzle Cavity on Resonance in Large SRM: Theoretical Modeling," *Journal of Propulsion and Power*, Vol. 18, No. 2, 2002, pp. 304–311. doi:10.2514/2.5935

[23] Anthoine, J., and Olivari, D., "Cold Flow Simulation of Vortex Induced Oscillations in a Model of Solid Propellant Boosters," AIAA Paper 99-

1826, 1999.
[24] Anthoine, J., Repellin, O., Buchlin, J.-M., and Olivari, D., "The Ariane-5 MPS Aeroacoustics Research at VKI: An Overview," *Proceedings of the 1st European Symposium on Launcher Technology*, Centre National d'Etudes Spatiales, Toulouse, France, 1999, pp. 569–578.
[25] Anthoine, J., Yildiz, D., and Buchlin, J.-M., "Nozzle Geometry Effect on the Instabilities in a Radial Injected Cold Flow Model of Solid Propellant Boosters," *Proceedings of the 2nd European Symposium on Launcher Technology, Space Solid Propulsion* [CD-ROM], Centre National d'Etudes Spatiales, Toulouse, France, 2000.
[26] Yildiz, D., Anthoine, J., and Buchlin, J.-M., "Influence Of Radial Injected Flow on the Aeroacoustic Coupling in Solid Propellant Boosters," AIAA Paper 2001-2101, 2001.
[27] Rockwell, D., and Naudascher, E., "Self-Sustained Oscillations of Flow Past Cavities," *Journal of Fluids Engineering*, Vol. 100, No. 2, 1978, pp. 152–165.
[28] Bruggeman, J. C., Hirschberg, A., van Dongen, M. E. H., and Wijnands, A. P. J., "Self-Sustained Aero-Acoustic Pulsations in Gas Transport Systems: Experimental Study of the Influence of Closed Side Branches," *Journal of Sound and Vibration*, Vol. 150, No. 3, 1991, pp. 371–393.
doi:10.1016/0022-460X(91)90893-O
[29] Flechter, N. H., and Rossing, T., *The Physics of Musical Instruments*, 2nd ed., Springer–Verlag, New York, 1998.
[30] Verge, M. P., Causé, R., Fabre, B., Hirschberg, A., Wijnands, A. P. J., and Steenbergen, A., "Jet Oscillations and Jet Drive in Recorder-Like Instruments," *Acta Acustica*, Vol. 2, No. 5, 1994, pp. 403–419.
[31] Rossiter, J. E., "Wind Tunnel Experiments on the Flow over Rectangular Cavities at Subsonic and Transonic Speeds," Aeronautical Research Council, Reports and Memoranda No. 3438, London, 1964.
[32] Hourigan, K., Welsh, M. C., Thompson, M. C., and Stokes, A. N., "Aerodynamic Sources of Acoustic Resonance in a Duct with Baffles," *Journal of Fluids and Structures*, Vol. 4, No. 4, 1990, pp. 345–370.
doi:10.1016/0889-9746(90)90130-W
[33] Gurevich, M. I., *Theory of Jets in Ideal Fluids*, Academic Press, New York, 1965.
[34] Anthoine, J., Mettenleiter, M., Repellin, O., Buchlin, J.-M., and Candel, S., "Influence Of Adaptive Control on Vortex Driven Instabilities in a Scaled Model of Solid Propellant Motors," *Journal of Sound and Vibration*, Vol. 262, No. 5, 2003, pp. 1009–1046.
doi:10.1016/S0022-460X(02)01034-9
[35] Lawrence, E. K., and Austin, R. F., *Fundamentals of Acoustics*, Wiley, New York, 1962.

K. Frendi
Associate Editor